Article

Gas Phase Structure and Reactivity of Doubly Charged Microhydrated Calcium(II)-Catechol Complexes Probed by Infrared Spectroscopy

Matias Butler, Pau Arroyo Mañez, Gabriela Cabrera, and Philippe Maitre

a) Intens. $\times 10^5$

148.0284
139.0229
□ [Ca(catechol)$_n$]$^{2+}$ (n=1-3)
● [Ca(catechol)(H$_2$O)$_n$]$^{2+}$ (n=1-4)
▲ [Ca(catechol)$_n$-H]$^+$ (n=1-2)
■ [Ca(catechol)$_2$(H$_2$O)$_n$]$^{2+}$ (n=1-2)
○ [Ca(catechol)(H$_2$O)$_n$-H]$^+$ (n=1-2)

185.0355
84.0048
102.0149
111.0273
65.9954
167.0015
259.0272

b) Intens. $\times 10^4$

148.0275
Intens.
3000
111.0173
111.0374
2000
1000
111.5215
112.0423
0
111.0
112.0
m/z

□ [Ca(catechol)$_n$]$^{2+}$ (n=1-3)
● [Ca(catechol)(H$_2$O)$_n$]$^{2+}$ (n=1-4)
▲ [Ca(catechol)$_n$-H]$^+$ (n=1-2)
■ [Ca(catechol)$_2$(H$_2$O)$_n$]$^{2+}$ (n=1-3)
○ [Ca(catechol)(H$_2$O)$_n$-H]$^+$ (n=1-2)

111.0318
130.0180
167.0012
185.0115
102.0144
139.0230
157.0326
203.0218

Figure 2
166x102mm (300 x 300 DPI)
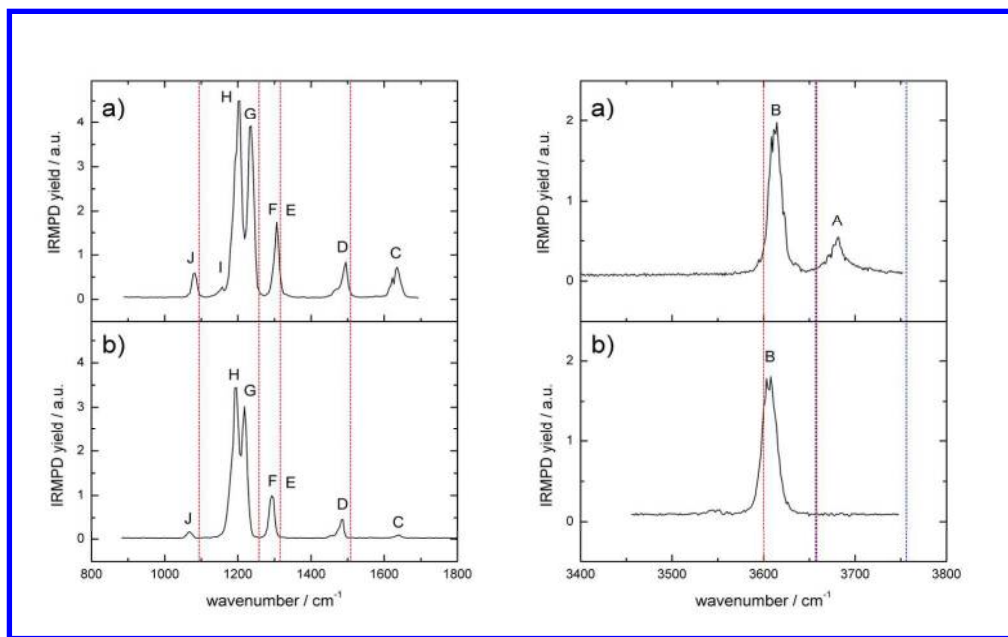
Figure 3
166x102mm (300 x 300 DPI)

Figure 4

1
2
3
4
5
6
7
8
9
10
11
12
13
14
15
16
17
18
19
20
21
22
23
24
25
26
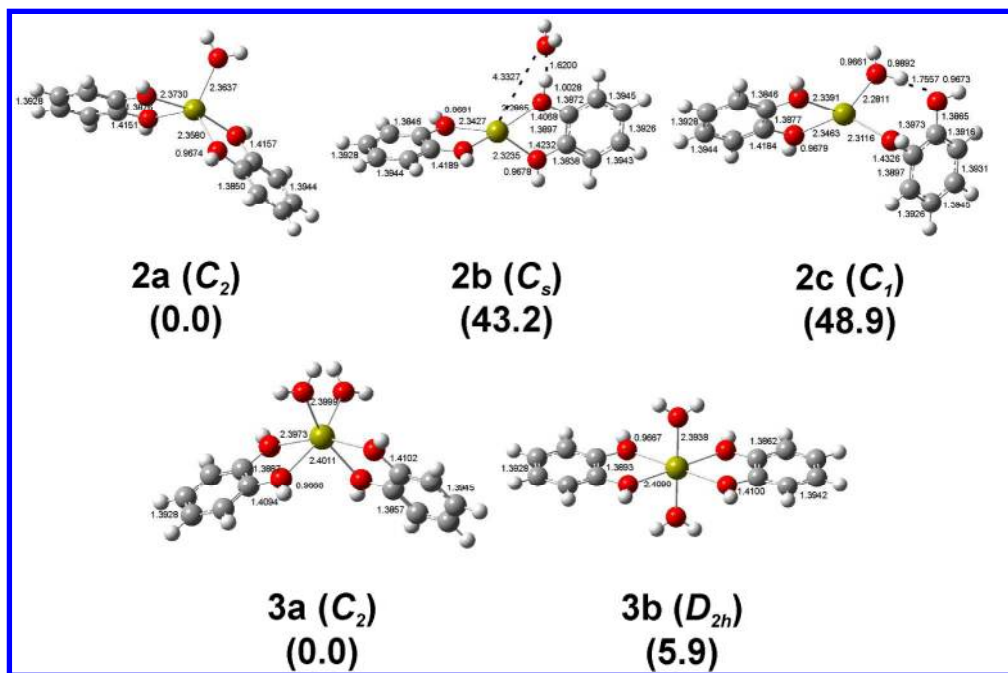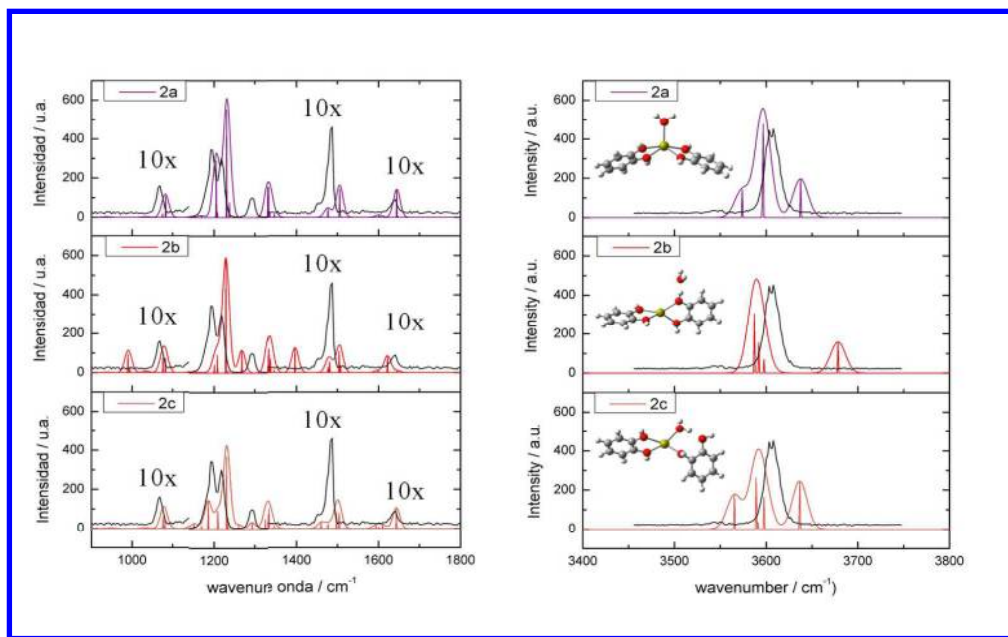
Figure 5
166x102mm (300 x 300 DPI)

27
28
29
30
31
32
33
34
35
36
37
38
39
40
41
42
43
44
45
46
47
48
49
50
51
52
53
54
55
56
57
58
59
60
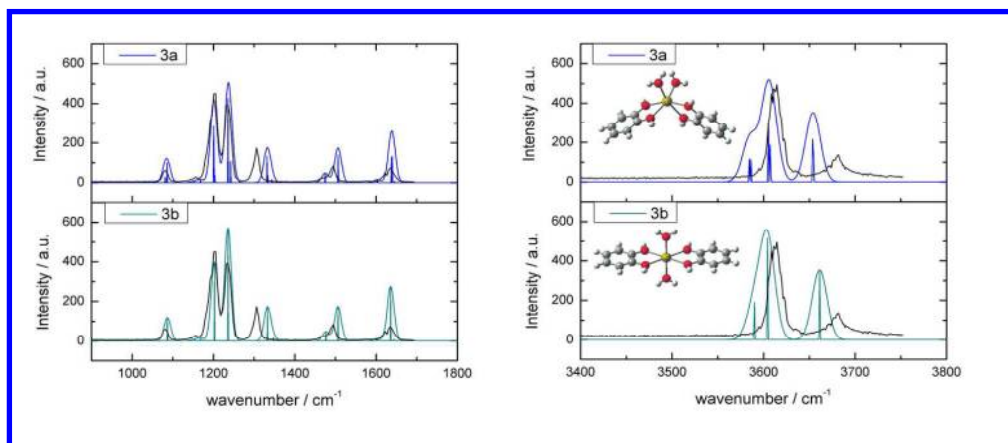
Figure 6
166x71mm (300 x 300 DPI)
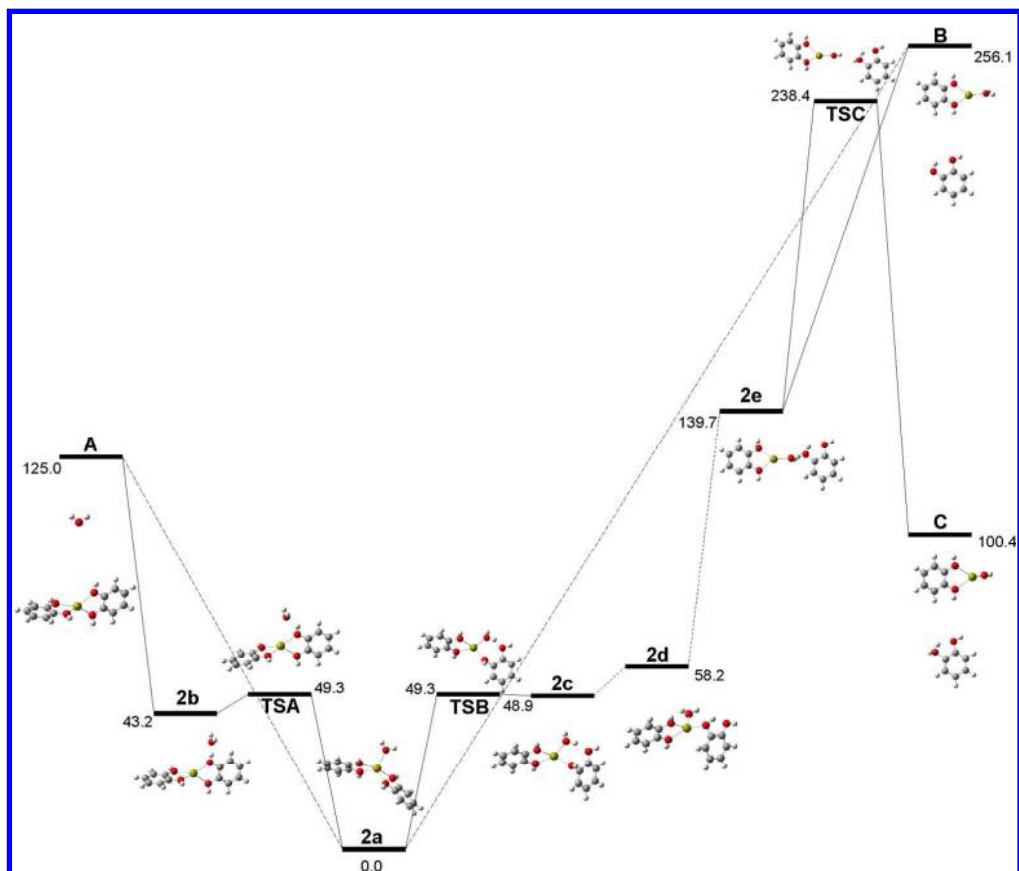
Figure 7
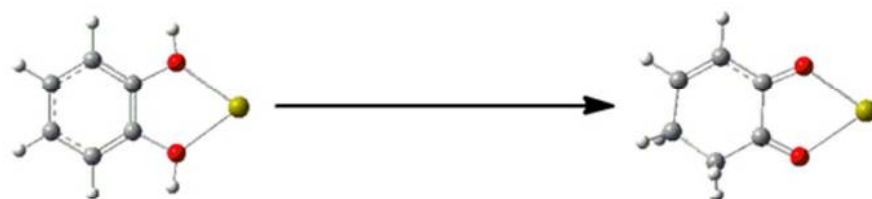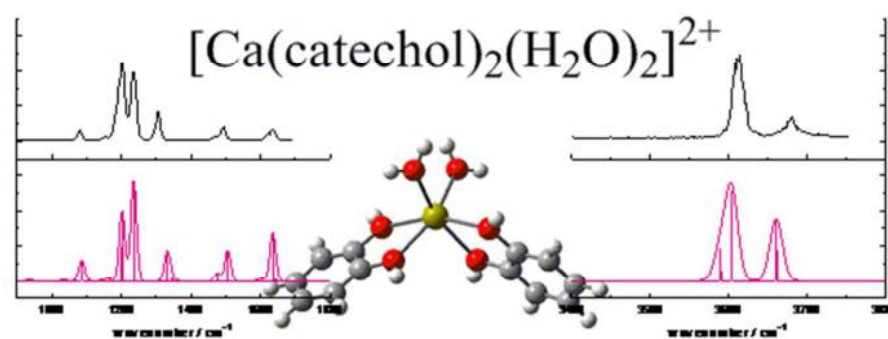
Table of content Graphic
51x44mm (300 x 300 DPI)

Gas phase structure and reactivity of doubly charged microhydrated calcium(II)-catechol complexes probed by infrared spectroscopy

Matias Butler[‡], Pau Arroyo Mañez[‡], Gabriela M. Cabrera[‡], Philippe Maître*[§]

[‡]Departamento de Química Orgánica, UMyMFOR-CONICET, Facultad de Ciencias Exactas y Naturales, Universidad de Buenos Aires, Ciudad Universitaria, Pabellón II, 3º piso, C1428EHA, Buenos Aires, Argentina.

[§]Laboratoire de Chimie Physique, Faculté des Sciences, Université Paris-Sud, UMR8000 CNRS, 91405 Orsay Cedex, France

Corresponding Author

* e-mail: philippe.maitre@u-psud.fr Tel: +33 (0) 1 69 15 32 50

Gas Phase Structure and Reactivity of Doubly Charged Microhydrated Calcium(II)-Catechol Complexes Probed by Infrared Spectroscopy

Doubly charged microhydrated adducts formed from catechol and calcium(II) were produced in the gas phase using electrospray ionization (ESI) appearing as the most important ions in the mass spectra recorded. The gas phase structures of $[Ca(catechol)_2(H_2O)]^{2+}$ and $[Ca(catechol)_2(H_2O)_2]^{2+}$ have been assayed by IR multiphoton dissociation (IRMPD) spectroscopy, recording their vibrational spectra in the 3450–3750 cm^{-1} range (OH stretching region) and in the 900–1700 cm^{-1} fingerprint spectral region. The agreement between experimental and calculated IR spectra of the selected cluster ions confirmed the suitability of the proposed geometries. In addition, quantum chemical calculations at the B3LYP/6-311+G(d,p) level of theory were performed for $[Ca(catechol)_2(H_2O)]^{2+}$ in order to gain insight into the major routes of dissociation. The results suggest that loss of the water molecule is the lowest energy fragmentation channel followed by charge separation products and neutral loss of one catechol molecule, in agreement with the product ions observed upon collision induced dissociation (CID).

KEYWORDS: Electrospray Ionization Mass Spectrometry (ESI-MS); metal adduct ions; IR multiphoton dissociation (IRMPD); collision induced dissociation (CID); ab initio quantum chemical calculations.

1. Introduction

Catechol (1,2-dihydroxybenzene or pyrocatechol) and its derivatives occur as intermediary metabolites during the degradation of naturally-occurring and synthetic aromatic compounds[1]. They are ubiquitous in biological chemistry acting as electron donors or complexing agents[2] and are known to be powerful chelators of transition metals[3]. As a result, numerous studies of catechol-metal interactions are described in the literature, in solution for Al(III)[4,5], in the solid state for Ag(I)[6], in solution and the solid state for Ni(II)[7], by quantum chemical calculations and studies in solution for Pb(II)[8] and by mass spectrometric methods and studies in solution for Fe(III)[9], just to mention some of the examples.

Interaction of catechol with Ca(II) has never been studied in the gas phase to the best of our knowledge, while there are recent studies in solution which have focused on the effect of calcium(II) on acid base and oxidation properties of catechol[10,11]. The potential of electrospray ionization (ESI) for obtaining and studying gas-phase metal complexes was realized soon after the method had been introduced by Fenn and co-workers as a soft-ionization technique for polar non-volatile molecules[12]. Complexation with metal ions in solution, followed by efficient transport of charged complexes to the gas phase by ESI, represents a promising method for ionization of a variety of analytes, including those that are not directly amenable to ESI. It is therefore interesting to investigate the coordination chemistry of calcium dication and catechol. Particularly, the coordination mode (mono or bidentate), whether this coordination induces or not keto-enol tautomerization and the coordination number of the metal are three points that must be elucidated.

Although structural information can be derived from Tandem Mass Spectrometry (MS/MS), the recent development of IR multiple photon dissociation (IRMPD) spectroscopy integrated to

ESI-MS/MS, in combination with quantum chemical calculations, has demonstrated to be an efficient tool to characterize the structure of gas-phase metal complexes[13-18]. In a scenario where numerous structures might account for ring hydrogen shifts[19] as well as metal binding sites[20], the use of IRMPD spectroscopy can provide direct structural information thus facilitating the assignment of the most relevant structures calculated with those observed in the mass spectra.

This work is part of ongoing investigations on the use of metal complexation combined with electrospray ionization mass spectrometry for the differentiation of isomeric compounds, such as hydroxypyridine *N*-oxides[21] and dihydroxyarenes[22]. We present herein a detailed study of the major calcium complexes formed with catechol in the gas phase using a combination of tandem mass spectrometry and IRMPD spectroscopy. IRMPD spectroscopy was used in the present work to investigate the gas-phase structures of mycrohydrated calcium(II) clusters with catechol, denoted $[Ca(catechol)_2(H_2O)]^{2+}$ and $[Ca(catechol)_2(H_2O)_2]^{2+}$, in combination with quantum chemical calculations at the B3LYP level of theory. The experiments are supported with theoretical calculations in order to achieve a better understanding of the major contributions to the observed features in the mass spectra obtained, including the characterization of the main ions obtained, their IRMPD spectra, and the analysis of the relative stability of their possible primary dissociation products.

2. Experimental and Theoretical Methods

Chemicals and sample preparation

Catechol was purchased from Sigma-Aldrich as a solid in analytical reagent grade and used without further purification. The stock solution was prepared by dissolving catechol in methanol (1 mM); $CaCl_2$ in water (1 mM) and mixing both solutions in a 1:1 ratio before infusion.

Mass spectrometry

Tandem Mass spectrometric analyses were performed using a Bruker micrOTOF-Q II hybrid quadrupole time-of-flight mass spectrometer (Bruker Daltonics, Billerica, MA, USA), equipped with ESI. The instrument was operated at a capillary voltage of 4.5 kV with an end plate offset of –500 V, using N_2 as nebulizer gas at 0.4 bar and as dry gas at 4.0 l min^{-1} and a dry temperature of 180 °C. The quadrupole mass filter was set with a 1.0 Da window for transmission (isolation) of precursor ions. Fragmentation of the mass-selected ions (collision-induced dissociation; CID) was performed in a radiofrequency-only quadrupole collision cell with ultra-high purity (UHP) Argon as collision gas. The collision cell was set to a collision energy of 6.0 eV with a gas flow rate at 5% of maximum and the cell RF was set at 100 Vpp.

Multi-point mass calibration was carried out using a sodium formate solution from *m/z* 50 to 900 in positive ion mode. Data acquisition and processing were carried out using the Bruker Compass Data Analysis ver. 4.0 software supplied with the instrument. Sample solutions were infused into the source using a KDS 100 syringe pump (KD Scientific, Holliston, MA, USA) at a flow rate of 3 μL min^{-1}.

Infrared (IR) spectroscopy analyses were performed using a 7 Tesla Fourier Transform Ion Cyclotron Resonance (FT-ICR) tandem mass spectrometer (Bruker Apex Qe) equipped with an Apollo II ESI ion source, a quadrupole mass filter, and a hexapole accumulation/collision cell. The solution was introduced in the source using direct infusion with a syringe pump at a flow rate of ~3 μL min^{-1}. Spray voltage of 4 kV and capillary temperature of 180 °C were used.

Infrared multiple photon dissociation

To obtain the IRMPD spectra of each cluster ion, these were first mass-selected in the quadrupole mass filter before injection into the ICR trap. The characteristic isotopic pattern of

the major doubly charged ions confirmed the proper ion identification and selection of $[Ca(catechol)_2(H_2O)]^{2+}$ and $[Ca(catechol)_2(H_2O)_2]^{2+}$ cluster ions. IRMPD spectroscopy of the gas-phase cluster ions was performed employing two experimental setups based on the coupling of the 7 Tesla hybrid FT-ICR tandem mass spectrometer with two IR lasers. For the IR spectroscopy of the selected cluster ions in the 900–1700 cm⁻¹ spectral range, the Infrared Free Electron Laser (IR FEL) from the Centre Laser Infrarouge d'Orsay (CLIO) was used. The experimental setup and its performance are described in details elsewhere[23].

The FEL was operated at 45 MeV to record IRMPD spectra with a nearly constant output power in the 900-1700 cm⁻¹ fingerprint range. The FEL output consists of 8 μs long macropulses at a repetition rate of 25 Hz. Each macropulse is composed of 500 micropulses, each a few picoseconds long. The laser wavelength was monitored with a monochromator coupled to a pyroelectric detector array. The spectral width (fwhm) was less than 0.5% of the central wavelength, which corresponds to 5 cm⁻¹ at 1000 cm⁻¹. The laser power varied between 400 and 600 mW in the frequency range of 800-1600 cm⁻¹, as measured before and after each scan.

IR spectra of the cluster ions in the 3450–3750 cm⁻¹ spectral range (OH stretching region) were recorded coupling the FT-ICR with an optical parametric oscillator/amplifier (OPO/OPA) laser system[24,25] (LaserVision, Bellevue, WA, USA). This laser system is pumped by an InnolasSpitlight 600 (München, Germany) non-seeded Nd:YAG (1064 nm, 550 mJ/pulse, bandwidth ~1 cm⁻¹) laser running at 25 Hz and delivering pulses of 4–6 ns duration. Typical output energy of the OPO/OPA was 12–13 mJ/pulse at 3600 cm⁻¹ with a 5 cm⁻¹ (fwhm) bandwidth.

The ions were irradiated in the ICR trap either by the IR-FEL or the OPO/OPA, for 0.25 s or 1-2 s, respectively. When the laser is tuned on resonance with a vibrational transition, multiple

photons are absorbed by mass-selected ions in a stepwise process eventually leading to the fragmentation[26]. By monitoring the intensities of parent (Iparent) and resulting fragment ions (Ifragment) as a function of the laser wavenumber, the IRMPD spectrum was obtained by plotting the IRMPD yield R = -ln(Iparent/[Iparent+Σ Ifragment]) as a function of the laser wavenumber. The only fragmentation channels observed upon IRMPD of $[Ca(catechol)_2(H_2O)]^{2+}$ and $[Ca(catechol)_2(H_2O)_2]^{2+}$ cluster ions correspond to the sequential loss of water molecules.

Geometry and frequency calculations

All calculations were performed using the Gaussian 03 computational package[27]. Quantum chemical calculations were carried out on the cluster ions to characterize the structure and energetics, as well as their infrared absorption spectra for band assignments. The characterization of the stationary points on the potential energy surface (PES) of these cluster ions was performed using the B3LYP[28,29] hybrid density functional theory (DFT) approach. This approach has been found to provide a good compromise between accuracy and computational cost in the cases of calcium complexes with formaldehyde[30], ammonia and water[31]. Calculations were performed with the 6-31+G(d,p) basis set and then all stationary points were re-optimized using the 6-311+G(d,p) basis set. These basis sets, featuring both polarized and diffuse orbitals, have been proved to be well suited for investigating similar systems using B3LYP[32].

Relative energies were computed using the B3LYP/6-311+G(d,p) optimized geometries including corrections for zero-point vibrational energy. Two basis sets (6-311+G(d,p) and 6-311+G(2d,2p)) were used to evaluate the energetics using the density functional approach (B3LYP) and also the post-Hartree Fock (MP2) approach.

The B3LYP/6-311+G(d,p) optimized structures were characterized by harmonic frequency analysis as local minima (all frequencies real) or first order saddle points (one imaginary

frequency). Harmonic vibrational frequencies for comparison with IRMPD spectra were scaled

by a factor of 0.98 and 0.95, in the fingerprint and the hydroxyl stretching regions, respectively.

These dual scaling factor values are similar to those previously determined to improve the

agreement between calculated and observed absorption frequencies[33]. Furthermore, it should also

be noted that similar scaling factor values have shown a satisfactory agreement between

experimental and theoretical IR absorption spectra for various gas phase molecular ions[24,34].

Theoretical IR stick spectra were convoluted with a Gaussian function with a width (fwhm) of 10

cm^{-1} in order to facilitate convenient comparison with the experimental spectra.

3. Results and Discussion

3.1 Formation and fragmentation of microhydrated calcium (II)-catechol complex ions

The ESI mass spectrum obtained from an equimolar (1 mM) mixture of catechol in methanol

and calcium chloride in water is shown in Figure 1a. Under the experimental conditions

employed, no ions were detected above *m/z* 300. Chlorine-containing or dimeric species were not

detected at a significant intensity while methanol containing cluster ions were identified at weak

abundances at low *m/z* values. Careful examination of the spectrum reveals the formation of both

singly- and doubly-charged ions.

The base peak of the spectrum corresponded to the dication $[Ca(catechol)_2(H_2O)_2]^{2+}$. Other

dications detected in high abundance corresponded to the series $[Ca(catechol)_x(H_2O)_y]^{2+}$ with

x=1-3 and y=0-4. Apart from doubly charged ions, three singly charged ions were detected,

albeit in low abundance. These belonged to the series $[Ca(catechol)_x(H_2O)_y–H]^+$, observed for

x=1-2 and y=0-1. See Table S1 in Supporting Information Section for more details about the

identity of the species with their measured *m/z* and error in ppm.
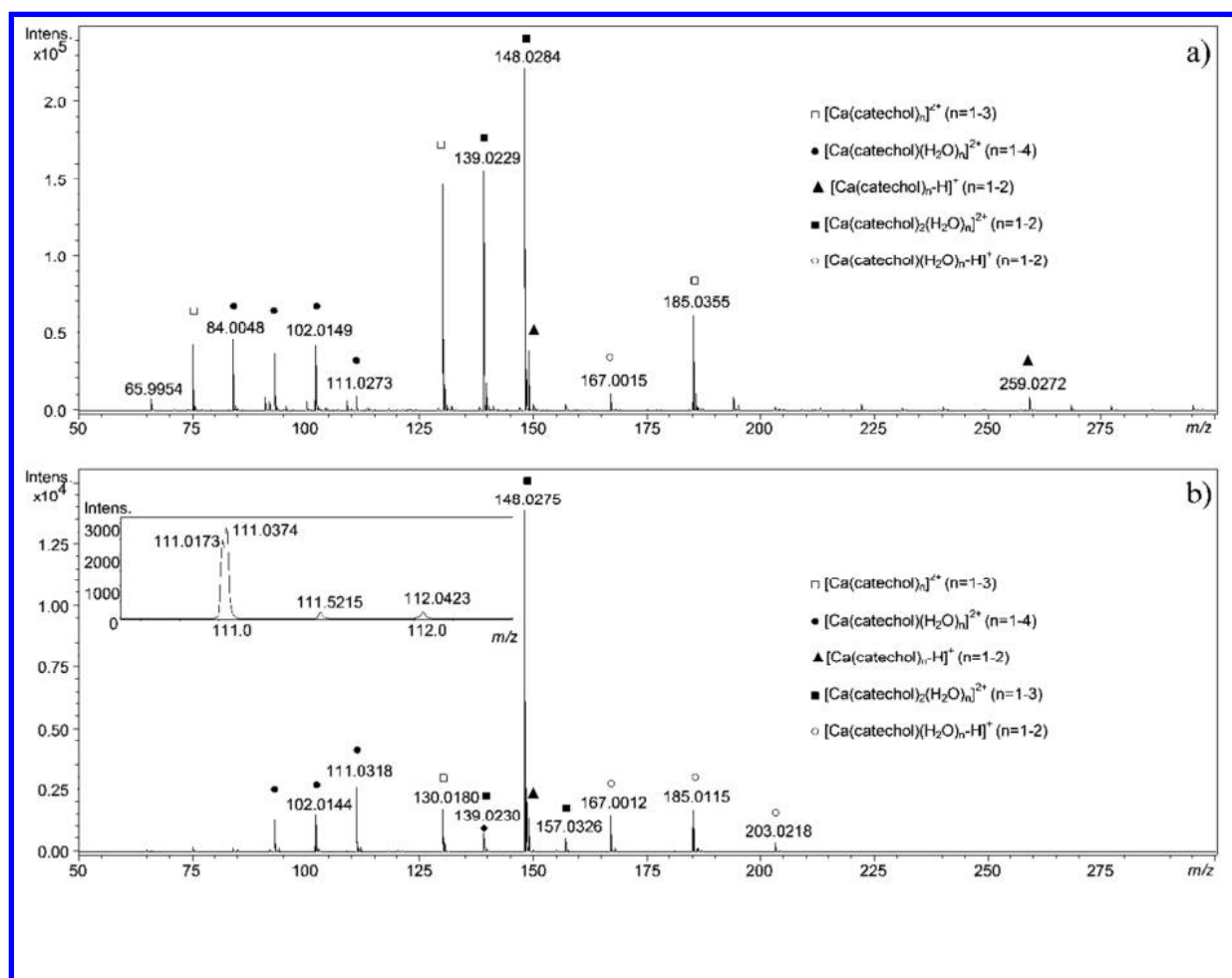
Figure 1. a) Positive electrospray spectrum of an aqueous $CaCl_2$/methanolic catechol (1 mM/1 mM) mixture. b) Low-energy CID spectrum of the $[Ca(catechol)_2(H_2O)]^{2+}$ adduct ion (*m/z* 139) recorded with a collision energy of 8 eV (laboratory frame).

Doubly charged calcium complexes have been readily generated by ESI for other ligands, such as methanol, pyridine[35], urea[36], thiourea[37], selenourea[38], formamide[39], glycine[40] and uracil[41], observing prominently dissociation by neutral ligand loss and proton transfer between ligands (charge separation) upon low energy CID conditions. With the aim of providing an insight into the dissociation pathways of the major ions observed in Figure 1a, $[Ca(catechol)_2(H_2O)]^{2+}$ (*m/z* 139) was mass selected. Its tandem mass spectra were recorded scanning the collision energy in the laboratory frame (Elab) from 5 to 11 eV, using argon as collision gas, which corresponds to

9

center-of-mass collision energies (ECM) ranging from 0.6 to 1.4 eV. The CID spectrum obtained at 8 eV (laboratory frame) is shown in Figure 1b. MS/MS spectra were recorded from m/z 50 up to m/z 300 although no fragment ions were detected above m/z 205. See Table S2 in Supporting Information Section for more details about the identity of the species with their measured m/z and error in ppm.
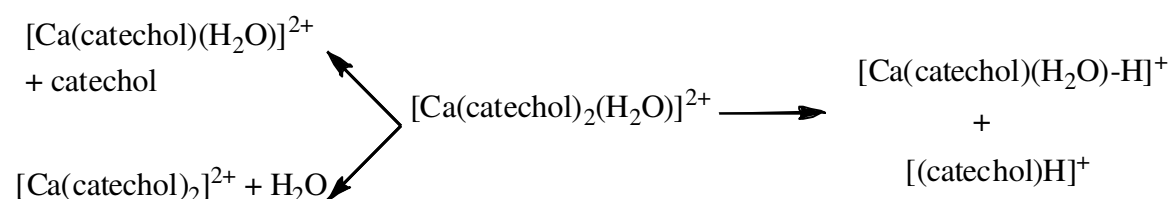
As can be seen in Figure 1b, doubly charged adduct ions with additional water molecules incorporated were actually observed besides the dications corresponding to neutral losses from the selected precursor ion. In addition, singly charged fragment ions assigned as $[(catechol)H]^+$ (m/z 111) and $[Ca(catechol)(H_2O)–H]^+$ (m/z 167) were detected, probably coming from a charge separation process. Similarly, incorporation of water molecules in the product ions (or the precursor ion) would lead to the remaining singly charged adduct ions observed in the tandem mass spectrum (Figure 1b). The presence of these adducts containing additional water molecules on the MS/MS spectrum might be imparted due to interaction of the complexes with trace amounts of water present in the collision cell coming probably from the Ar line[42]. Apart from these artifacts, the tandem mass spectra of the doubly-charged complex revealed two types of dissociation processes, leading either to new dications by neutral losses, or to singly charged species, through charge separation processes (See Scheme 1).

Scheme 1. Possible dissociation mechanisms from the adduct ion $[Ca(catechol)_2(H_2O)]^{2+}$.

$[Ca(catechol)(H_2O)]^{2+}$
+ catechol

$[Ca(catechol)_2(H_2O)]^{2+}$ ⟶

$[Ca(catechol)(H_2O)-H]^+$
+
$[(catechol)H]^+$

$[Ca(catechol)_2]^{2+} + H_2O$

High mass resolution allowed for differentiating and unambiguously identifying two ions of similar intensity in the vicinity of *m/z* 111.0 and *m/z* 185.0. The first case is shown in the inset of Figure 1b, where singly charged protonated catechol, [M+H]$^+$, is exhibited along with a doubly charged ion, [M+Ca+4H$_2$O]$^{++}$. The second case becomes evident when comparing Figure 1a and 1b, noticing the doubly charged ion, [3M+Ca]$^{++}$, and the singly charged ion, [M+Ca+2H$_2$O-H]$^+$ detected, respectively,

The dissociation pathways observed were further studied by theoretical calculations to gain a better understanding on the energetics involved in the former processes (see section 3.4). Before the discussion of the dissociation pathways of these cluster ions, we will first discuss their structures by comparing IRMPD and calculated IR absorption spectra of the low lying isomers.

3.2 Gas phase Infrared Spectroscopy of Ca(II)/catechol complexes

Neutral catechol ligand: vibrational analysis

In both the 800-2000 cm^{-1}, *i.e.* fingerprint region, and 3000-3800 cm^{-1} spectral region, where the O-H stretching vibrational modes are found, catechol shows IR absorption bands. Slight spectral shifts characteristic of the coordination mode and/or coordination number are expected upon complexation to Ca(II). It is thus useful to characterize the performance of the theoretical method for describing the IR absorption spectrum of bare neutral catechol in the first place. Particularly, comparison of predicted and experimental spectra could confirm the appropriateness of using one scaling factor for each of the two regions.

The experimental IR spectrum of catechol in the gas phase (Figure 2) was taken from the NIST database[43], and the measured band frequencies (labeled A-J), as well as their assignments, are listed in Table 1. Some assignments were taken from former catechol studies[44], whereas others were adapted from recent revised literature using the Wilson notation[45] for monosubstituted

benzene derivatives. The calculated IR spectra of the two lowest energy conformers **1a** and **1b** of

catechol are shown in Figure 2. Both calculated structures are planar. The lowest energy

conformer **1a** is characterized by an orientation where one of the hydroxyl groups is pointing

towards the other, albeit without hydrogen bond interaction, according to the studies available in

the literature[46,47].
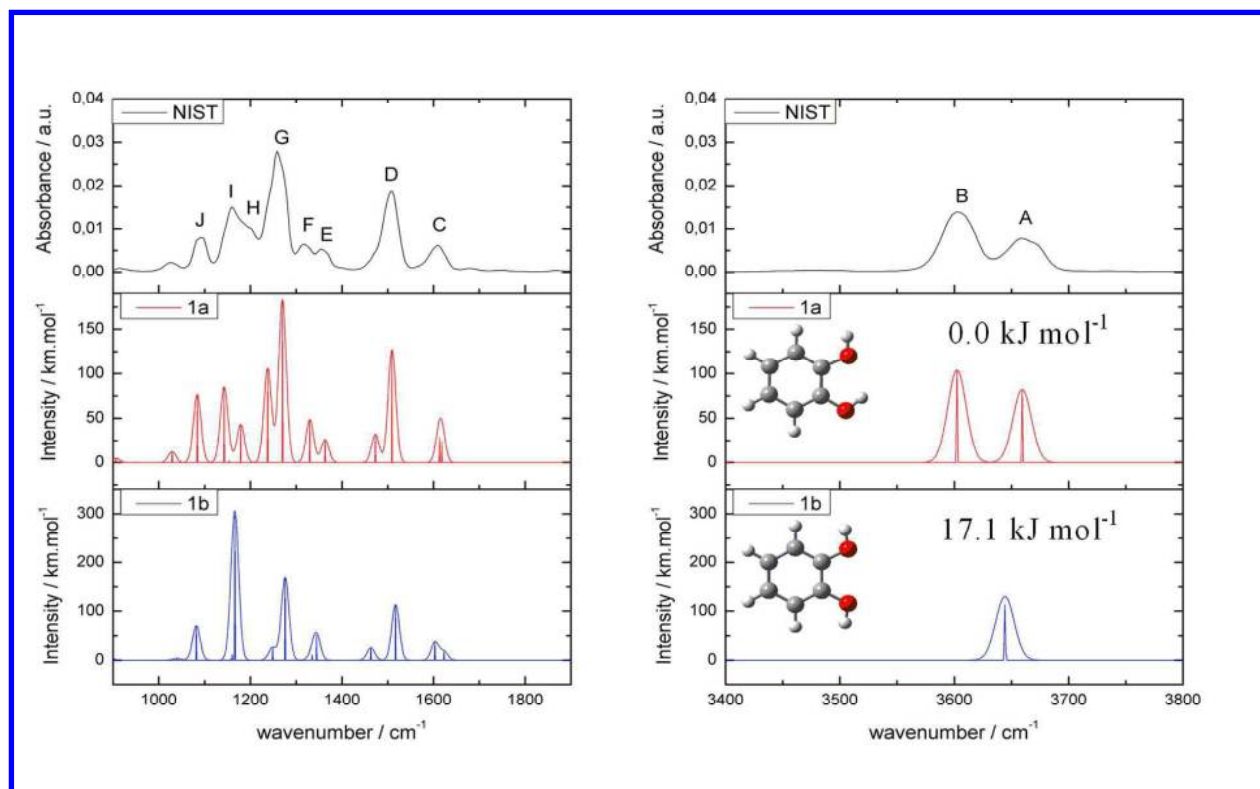
Figure 2. Comparison of the gas phase IR spectrum of catechol taken from the NIST spectral

database[43] to the linear IR spectra predicted for the two most stable conformers of neutral

catechol at the B3LYP/6-311+G(d,p) level of theory. Relative energies are given in kJ mol^{-1}.

Overall, the experimental spectrum better match with the predicted IR absorption spectrum of

the lowest energy structure **1a**. In particular, the observed splitting of the O-H stretching bands,

A and B (Figure 2), is a clear signature of the lowest energy conformer **1a**. It should be noticed

that the observed frequency splitting (56 cm^{-1}) is well reproduced by the theoretical procedure

employed (57 cm^{-1}). Two other bands observed at 1158 (I) and 1316 cm^{-1} (F) are also

characteristic of the conformer **1a**. They are also well predicted at the B3LYP/6-311+G(d,p)

level of theory. Two bands are predicted at 1143 and 1330 cm^{-1}, and are assignable to the

bending modes of C-H and C-O-H (β_{CH} and β_{COH}, respectively). These modes might be useful

features to differentiate between the two conformations when catechol is bound to Ca(II). It can

be noticed that conformer **1b**, lying 17.1 kJ mol^{-1} higher in energy than the conformer **1a**,

displays two sharp bands at 1166 and 1276 cm^{-1} which are such that **1b** does not match the

experimental spectrum. Moreover, assuming a Boltzmann distribution and from the relative free

energies calculated in the gas phase at room temperature (298.2 K), the relative abundance of

conformer **1b** in equilibrium with **1a** is expected to be less than 0.1%.

   As can be seen in Table 1, the IR spectral properties of conformer **1a** of catechol determined at

the B3LYP/6-311+G(d,p) level are in good agreement with the experimental values, the mean

difference between experimental and scaled frequencies being ~9 cm^{-1}. In the fingerprint range,

all theoretical frequencies agree to within 20 cm^{-1} with the available experimental values using a

scaling factor value of 0.98. In the OH stretching region, a scaling factor value of 0.95 leads to

an excellent agreement with the observed frequency values. Besides, the widths (fwhm) of

isolated transitions in the experimental spectrum taken in a GC/MS/IRD[43] are typically 20 cm^{-1}

and some features were not well resolved.

Table 1. Experimental vibrational frequencies of catechol[43] compared to values of the conformers

calculated at the B3LYP/6-311+G(d,p) level of theory. Harmonic frequencies scaled by 0.98 in

the fingerprint range and by 0.95 in the OH stretching range.

vibrational mode[a]	1b[b] ν_{calc}/ cm^{-1}	1a[b] ν_{calc}/ cm^{-1}	catechol[c] ν_{exp}/cm^{-1}	$\Delta\nu$ (ν_{exp}-ν_{calc}(1a)) /cm^{-1}

σ_{OH}	3644 (113)	3659 (82)	3658 A	-1
σ_{OH}	3645 (17)	3602 (104)	3602 B	0
σ_{CC} (ν_{9a})	1623 (18)	1618 (24)	1608 C	-10
σ_{CC} (ν_{9b})	1603 (37)	1613 (28)		-5
σ_{CC} (ν_{18b})	1517 (113)	1509 (127)	1508 D	-1
σ_{CC} (ν_{18a})	1463 (25)	1473 (32)		
σ_{CC} (ν_{15})	1345 (51)	1363 (26)	1354 E	-9
β_{COH}	1335 (11)	1330 (49)	1316 F	-14
σ_{CO} (C_1-O_1)	1276 (169)	1270 (183)	1258 G	-12
σ_{CO} (C_2-O_2)	1249 (26)	1238 (106)		20
β_{COH}	1166 (296)	1179 (43)	1190 H	11
β_{CH} (ν_{8b}) β_{OH}		1143 (84)	1158 I	15
β_{CH} (ν_{19a}) β_{OH}	1082 (70)	1084 (76)	1094 J	10

[a]All modes are in-plane vibrations according to the Wilson notation (**ν_{ni}**) adapted for monosubstituted benzene molecules with C_{2V} symmetry consistently assigned in Ref. 45. Assignments of vibrational frequencies taken from Refs. 44 and 45.

[b]Calculated IR intensities in km.mol^{-1} are given in parentheses.

[c]Peak positions from the spectrum in Fig. 2 taken from the NIST database from Ref. 43.

IRMPD Spectra of microhydrated calcium complexes

The IRMPD spectra of [Ca(catechol)$_2$(H$_2$O)]$^{2+}$ and [Ca(catechol)$_2$(H$_2$O)$_2$]$^{2+}$ cluster ions in the fingerprint spectral range (950-1700 cm^{-1}) and in the O-H stretching modes region (3450–3750 cm^{-1}), are shown in Figure 3. Only loss of water molecules was observed as a consequence of IR absorption in all recorded spectra. When comparing the IRMPD spectra of the two cluster ions shown in Figure 3, it can be noticed an almost identical profile with bands slightly red-shifted

from $[Ca(catechol)_2(H_2O)_2]^{2+}$ to $[Ca(catechol)_2(H_2O)]^{2+}$. However, the absence of band A in Figure 3b can be noticed.

On the basis of recent gas-phase IR spectroscopic investigations of water solvated metal cations, a first interpretation of these features can be made. Coordination of water to a metal cation induces a red-shift of the symmetric (ν_{sym}) and asymmetric (ν_{asym}) O-H stretches with respect to their positions (3657 and 3756 cm^{-1}, respectively)[48] for the free water molecule. This red shift evidenced for numerous metal hydrated systems[49,50] can be understood as resulting from a partial electron-transfer from the water molecule to the metal cation[51].
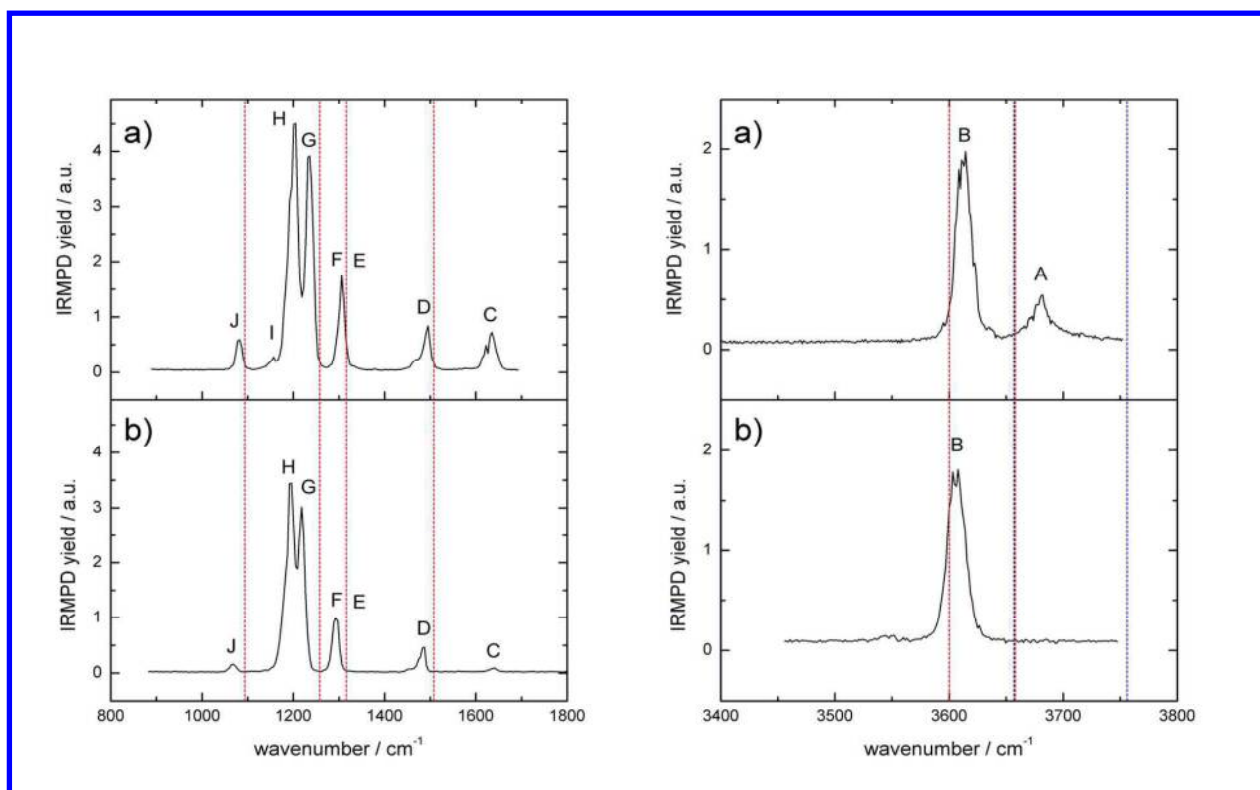
Figure 3. IRMPD spectra of a) $[Ca(catechol)_2(H_2O)_2]^{2+}$ and b) $[Ca(catechol)_2(H_2O)]^{2+}$ recorded in the fingerprint range and O–H stretching region. "Band labels" are those used for catechol, see also Tables 1-2. The dashed red lines correspond to some of the free catechol absorption bands shown in Figure 2, whereas the blue ones to the symmetric and assymetric stretches of the free water molecule.

Upon addition of several water molecules and approaching the maximum coordination number (CN) of the metal, which has been shown to be 6 in the gas phase[52], competition between direct coordination to the metal cation and formation of water–water hydrogen bonds can be anticipated. For $Ca(H_2O)_n^{2+}$ metal dication, there is no evidence for hydrogen bond formation associated with a second shell of water molecules for $n \leq 6$. The appearance of a wide band at frequencies lower than 3500 cm^{-1} in the IR spectrum for $Ca(H_2O)_7^{2+}$, having been interpreted as the result of the formation of structures with hydrogen bonds between first and second shell water molecules[52]. From $n = 1$ to 6, a progressive decrease of the red-shift of the ν_{sym} and ν_{asym} bands of $Ca(H_2O)_n^{2+}$ was observed, which is consistent with decreased charge transfer from any given water molecule to the metal ion, at higher coordination number.

The same arguments as discussed above also apply for the hydroxyl stretching modes σ_{OH} of the catechol ligands coordinated to the metal cation. Analogously, as additional ligands interact with the metal, one can expect that the electronic transfer from each ligand to the metal dication decreases, thus decreasing the spectral red shifts of the IR bands of the ligands.

Taking into account the arguments afore mentioned, and anticipating red shifts of the vibrational modes in the O-H stretching region, the band A in Figure 3a can be tentatively assigned to ν_{asym} mode of vibration of water molecules coordinated to the metal ion. On the other hand, the band B can be assigned to the ν_{sym} mode of vibration of the water molecule coordinated to the metal ion as well as to the hydroxyl stretching modes σ_{OH} of the catechol ligands.

As mentioned above, the asymmetric band of the water molecule could not be observed in the IRMPD spectrum of $[Ca(catechol)_2(H_2O)]^{2+}$. Furthermore, as can be seen in Figure 3b, band B is observed to be more intense than band A. Similar observations have already been made with other solvated metal systems[49], and also solvated proton[53]. For example, in the case of solvated

$Ca(H_2O)_n^{2+}$ ions[52], the asymmetric water stretching was not observed for n= 4 and n=5, becoming discernible only for n=6 at ~3670 cm^{-1}. An interpretation has been proposed based on the mechanical view of the intramolecular vibrational redistribution (IVR)[54].

The band labels C-J employed for bare catechol (Table 1), are used to identify and tentatively assign the distinct bands exhibited in Figure 3 a) and b). The band frequencies along with their assignments are listed in Table 2. Assuming that the coordination to Ca(II) occurs through the oxygen atoms of catechol, it is expected that the major vibrational shifts are associated with the vibrational modes of catechol involving these atoms. From the vibrational analysis of catechol, it can thus be inferred that the most relevant ones for the structural characterization are those assignable to the stretching (G) and bending modes (E, F, H) of the C-O ($\boldsymbol{\sigma_{CO}}$ and $\boldsymbol{\beta_{COH}}$, respectively) in contrast with the stretching modes of C-C ($\boldsymbol{\sigma_{CC}}$) and bending modes of C-H ($\boldsymbol{\beta_{CH}}$). Here, the major red-shift from the bare neutral catechol occurs for the band labeled G (assigned to C-O stretching mode $\boldsymbol{\sigma_{CO}}$). In order to confirm the vibrational assignment of the transitions observed in the IRMPD spectra, quantum chemical calculations were performed.

Table 2. Experimental vibrational frequencies of catechol[43] compared to $[Ca(catechol)_2(H_2O)_2]^{2+}$ and $[Ca(catechol)_2(H_2O)]^{2+}$ cluster ions.

vibrational mode[a]	$[Ca(catechol)_2(H_2O)_2]^{2+}$ ν_{exp}[b] /cm^{-1}	$[Ca(catechol)_2(H_2O)]^{2+}$ ν_{exp}[b] /cm^{-1}	catechol ν_{exp}[c] /cm^{-1}
ν_{bH2O}	1636 [17] C	1646 [12] C	
σ_{CC} (ν_{9a})			
σ_{CC} (ν_{9b})			1608 C
σ_{CC} (ν_{18b})	1495 [20] D	1489 [10] D	1508 D
σ_{CC} (ν_{18a})			
σ_{CC} (ν_{15})			1354 E

β_{COH}	1306 [18] E,F	1300 [15] E,F	1316 F
σ_{CO}	1234 [18] G	1225 [16] G	1258 G
β_{COH}	1203 [20] H	1198 [17] H	1190 H
β_{CH} (ν_{8b}) β_{OH}	1157 I		1158 I
β_{CH} (ν_{19a}) β_{OH}	1080 [15] J	1071 [10] J	1094 J

[a] All modes are in-plane vibrations according to the Wilson notation (**ν_{ni}**) adapted for monosubstituted benzene molecules with C_{2V} symmetry consistently assigned in Ref. 45.

[b] Widths (in cm^{-1}) of the peaks are given in brackets.

[c] Peak positions from the spectrum in Fig. 2 assigned according to Ref. 45 and 44.
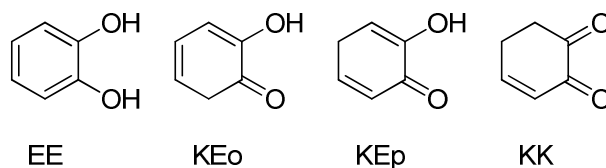
3.3 Structures of microhydrated calcium (II)-catechol clusters

Previously reported IR spectroscopic investigations of bare catechol[44] and catechol derivatives such as dopamine[55], as well as calcium(II) water clusters[52] provide a useful guide for the present calculations. An exhaustive exploration of the potential energy surface of the cluster ions is beyond the scope of this paper. Our goal is rather to determine the infrared signature of the different bonding motifs expected for these cluster ions. In this respect, the occurrence of tautomers had to be taken into account in the IRMPD spectra of Pb(II)-nucleobases complexes generated by ESI[56].

Recently, it has been reported[57] that the two *dienol* tautomers of catechol (**1a** and **1b**) were always lower in energy (differences higher than 60 kJ mol^{-1}) than the other *keto* species, predominating both in the gas phase and in solution, as shown by computational studies at the B3LYP/6-311++G(d,p) level of theory. This predominance was attributed to loss of aromaticity

stabilization in the *keto* forms. Starting from the aromatic dienol tautomer, which will be denoted as

EE, two low-energy keto-enol tautomers should be considered (Scheme 2). These two tautomers,

denoted as KEo and KEp, differ by the position of the CH_2 group. Only one diketo tautomer, denoted

as KK, corresponding to the maximization of π-conjugation, should be considered.

Scheme 2. Possible low energy tautomers of catechol.

EE   KEo   KEp   KK

Considering that large binding energies are expected to a dication, binding of catechol to Ca(II)

may be sufficient to induce *keto-enol* tautomerization. As an initial approach to the structures of

microhydrated calcium(II)-catechol clusters, complexes consisting of a single catechol ligand

coordinated to the metal cation were considered. This simplification aimed to examine and

compare structures featuring different coordination number as well as possible tautomers of the

ligand.

The optimized structures of the complexes along with their relative energies and calculated IR

spectra can be found in the Supporting Information section (Figure S1). Comparison of the IR

spectra (Figure S1) with the IRMPD spectra obtained for the cluster ions (Figure 3) revealed the

structure containing the catechol, *i.e.* the dienol EE tautomer, coordinated to the metal in a

bidentate fashion and in a conformation as that shown for **1b** (Figure 1) as the best candidate.

Structures containing *keto*-tautomers of catechol can be dismissed, in principle, due to the lack of

bands evidencing a C=O stretching mode which should appear as sharp peaks in the 1500-1700

cm^{-1} region in the IRMPD spectra.

Inspection of the relative energies of the four structures of the Ca(catechol)$^{2+}$ complex, corresponding to the coordination of the EE, KEo, KEp, and KK tautomers, reveals a drastic difference between B3LYP and MP2. As can be seen in Table 3, for Ca(catechol)$^{2+}$, the EE isomer is predicted to be significantly higher in energy than the isomers containing a keto-enol of di-keto tautomers at the B3LYP/6-311+G(d,p) level of theory. Extending the basis set to 6-311+G(2d,2p) does not significantly change the relative energies of these four structures of Ca(catechol)$^{2+}$. Basis set superposition effects (BSSE) are very similar (~1 kJ/mol per binding oxygen) for the four binding modes at this level of theory. Relative energies evaluated using the MP2 approach, however, are drastically different. Overall, the relative energies of the keto containing isomers do not change significantly from B3LYP to MP2. The EE containing isomer, however, is strongly stabilized. Two structures, corresponding to the coordination of the EE and KEp tautomers, were found to be nearly degenerate using the two basis sets at the MP2 level. As for the MP2 level, the BSSE corrections to the binding energies are found to be nearly the same for the four tautomers.

Table 3. Relative energies (in kJ mol^{-1}) of Ca(catechol)$^{2+}$ cluster ions calculated at the B3LYP and MP2 levels of theory. Basis set superposition effect (BSSE) corrections are shown in brackets.

Structure	B3LYP/	MP2/	B3LYP/	MP2/
	6-311+G(d,p)		6-311+G(2d,2p)	
EE	34	0	40 [1.7]	3 [6.1]
KEo	18	24	19 [1.7]	22 [6.3]
KEp	0	3	0 [1.6]	0 [6.3]

KK	13	18	11 [1.5]	18 [6.2]

Considering the above results for single catechol calcium complexes, one additional catechol ligand and the water molecules were incorporated to generate candidate structures for the mono and dihydrated calcium catechol clusters. On the basis of earlier reported studies of water solvated metal ions such as calcium[52,58] and magnesium[59,60] , the different bonding motifs characterizing the arrangement of the water molecules can be anticipated. Structures with trigonal, tetrahedral, square-pyramidal or octahedral geometries might be expected with calcium coordination number (CN) 3, 4, 5 or 6, respectively. Overall, the EE containing tautomers were found to be the lowest in energy at the MP2 level for the naked, mono- and di-hydrated $Ca(catechol)_2^{2+}$ complexes. At the B3LYP level, however, KE containing tautomers were predicted to be lower in energy for the naked and mono-hydrated $Ca(catechol)_2^{2+}$ complexes. The energy splitting between the EE and the KE containing isomers decreases when increasing the coordination number CN. Besides, in the case of the di-hydrated $Ca(catechol)_2^{2+}$ complex, the EE containing isomer is predicted to be the lowest in energy at the B3LYP level. The enolic tautomers were also shown to be stabilized upon association with calcium for uracil and related compounds[61].

Under our experimental conditions, on the basis of the study of multiple systems, it can be expected that only the lowest energy gas phase isomer is observed. Few exceptions confirm the rule. In particular, IR signature of multiple isomers have been observed in the case of protonated uracil, for example, being shown that the corresponding tautomers were nearly degenerate[62]. Since no IR signature of the C=O carbonyl stretch could be observed for the $Ca(catechol)_2(H_2O)_2^{2+}$ nor for the $Ca(catechol)_2(H_2O)_2^{2+}$ complexes, it may be thus concluded

21

that only isomers containing EE catechol tautomers were formed under our experimental conditions.Several structures containing one or two water molecules of coordination differing in the CN of calcium owe to the coordination mode of the catechol ligands, *i.e.* monodentate or bidentate were investigated. The most stable geometries of $[Ca(catechol)_2(H_2O)_n]^{2+}$ (n=1,2) complexes (**2a** and **3a**, respectively) were found to correspond to structures in which the water molecules are directly bound to Ca(II) with both catechol ligands coordinated in a bidentate fashion, thus maximizing the CN of the metal (Figure 4). For n=1, structures exhibiting an interligand hydrogen bond between the water molecule and a hydroxyl moiety (1.62 A and 1.76 A, respectively) were also considered. These structures (**2b** and **2c**) are predicted to be significantly higher in energy. It thus seems that the hydrogen bond formation does not compensate the decrease of the CN of Ca(II) from five (in **2a**) to four. In addition, hydrogen bonding interaction should lead to red-shifting of the OH stretching band, which was not observed experimentally. For n=2, two structures leading to a CN of six but differing in the configuration of the ligands were characterized. The Ca-O bond lengths of these structures are essentially similar (Figure 4). The lowest energy optimized structure (**3a**, C_2 symmetry) can be considered as a distorted octahedral geometry where the two water molecules are adjacent to each other, thus being the *cis* isomer. The *trans* isomer (**3b**, D_{2h} symmetry) is predicted to be slightly higher in energy.
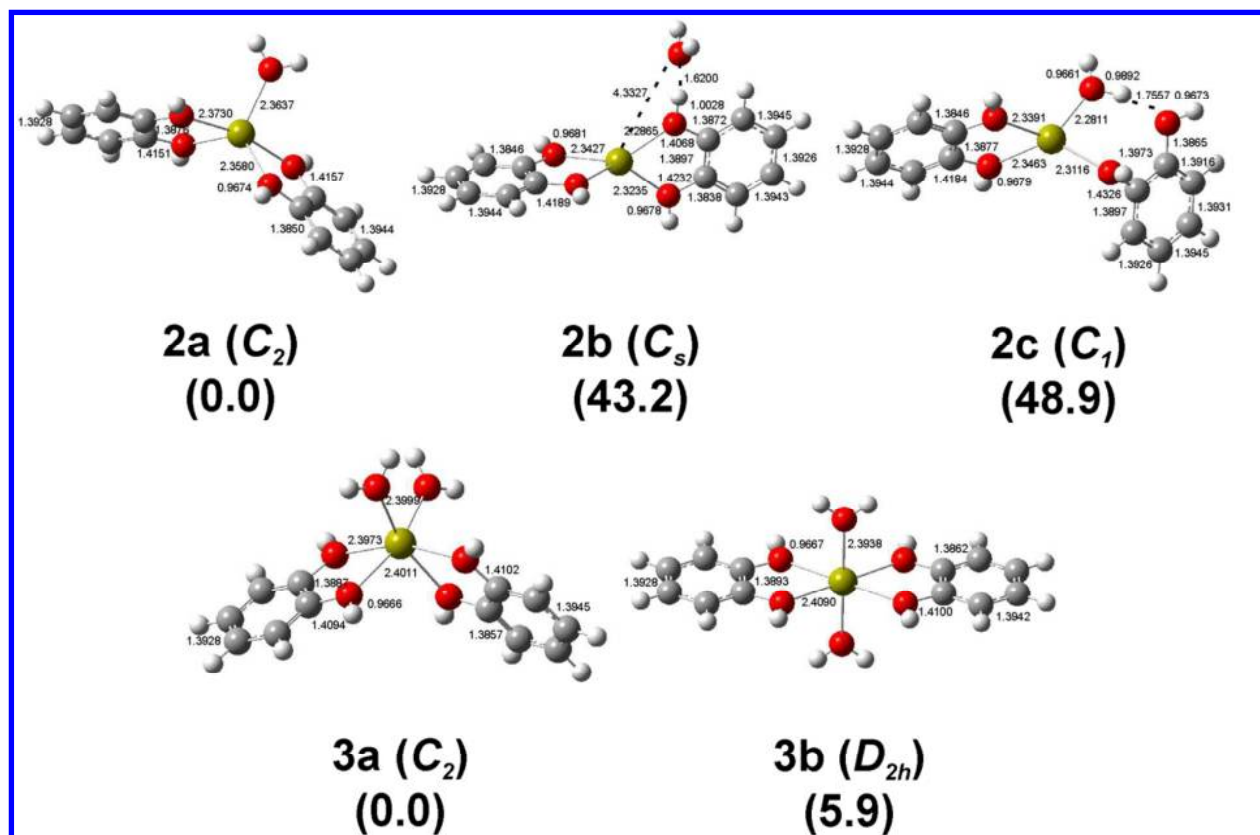
Figure 4. Structures (with symmetry point groups) of doubly charged bis-catechol calcium water adducts $[Ca(catechol)_2(H_2O)]^{2+}$ and $[Ca(catechol)_2(H_2O)_2]^{2+}$ optimized at the B3LYP/6-311+G(d,p) level of theory. Relative energies at 0K (shown in parentheses) are in kJ mol^{-1}; bond lengths are in angstroms.

Despite its multiple photonic nature, the IRMPD spectrum predominantly reflects the absorption of the first IR photon[26]. This observation justifies a comparison of the experimental IRMPD spectrum with a calculated linear one-photon IR absorption spectrum. Experimental IRMPD spectra of $[Ca(catechol)_2(H_2O)]^{2+}$ and $[Ca(catechol)_2(H_2O)_2]^{2+}$ are compared with IR linear spectra of the most relevant structures considered in Figures 5 and 6, respectively.From the comparison with the calculated spectra, the features predicted for structure **2a** (Figure 5) reproduce well the experimental IRMPD spectra of $[Ca(catechol)_2(H_2O)]^{2+}$, also being the most favored structure based on its relative energy with respect to **2b** and **2c**. On the other hand,

structures **3a** and the slightly less stable **3b** have essentially the same IR spectrum which fits well

with that of $[Ca(catechol)_2(H_2O)_2]^2$. As expected, no difference between these *cis/trans* isomers

could be found in the 1000-4000 cm^{-1}, where the bands are associated with the ligands

vibrational modes. Only a scan at lower frequencies, *i.e.* in the metal-ligand region may have

been conclusive.
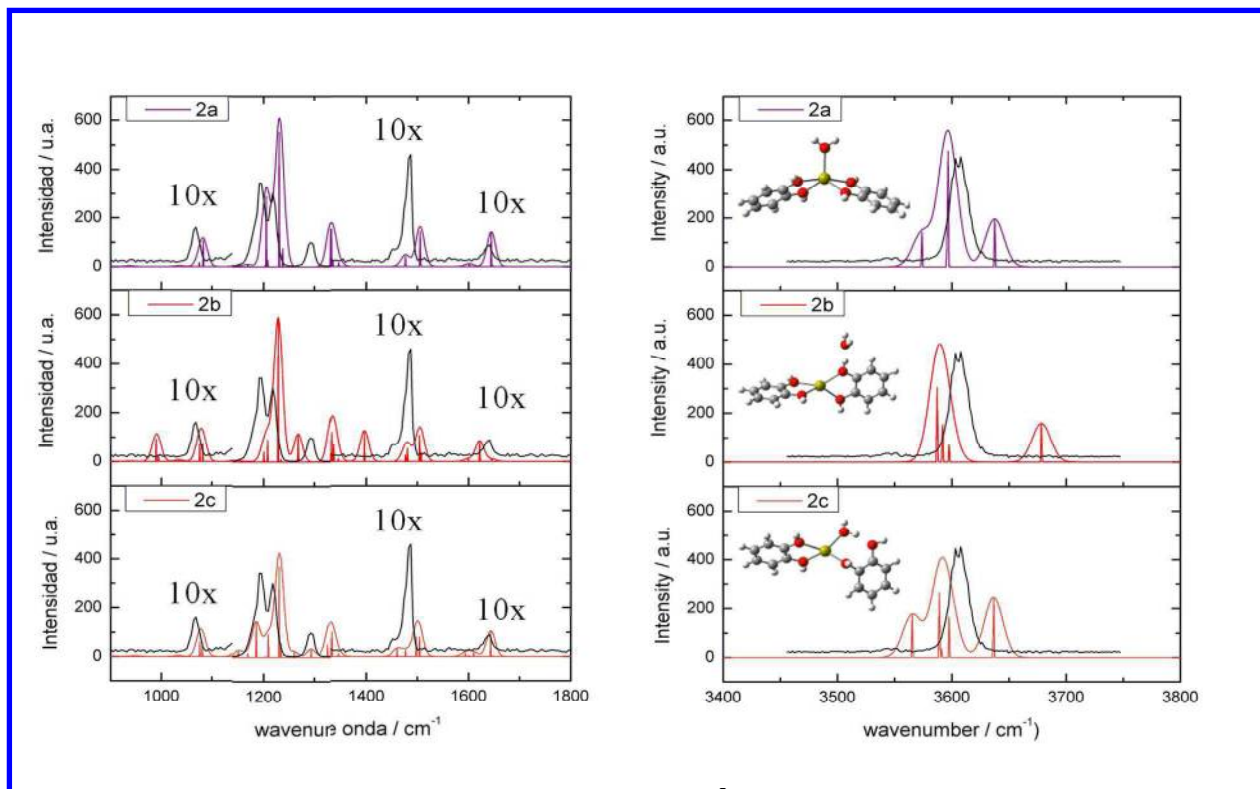
Figure 5. IRMPD spectra of $[Ca(catechol)_2(H_2O)]^{2+}$ (in black) compared with linear IR
absorption spectra of various structures evaluated at the B3LYP/6-311+G(d,p) level.

Figure 6. IRMPD spectra of $[Ca(catechol)_2(H_2O)_2]^{2+}$ (in black) compared with linear IR absorption spectra of various structures evaluated at the B3LYP/6-311+G(d,p) level.
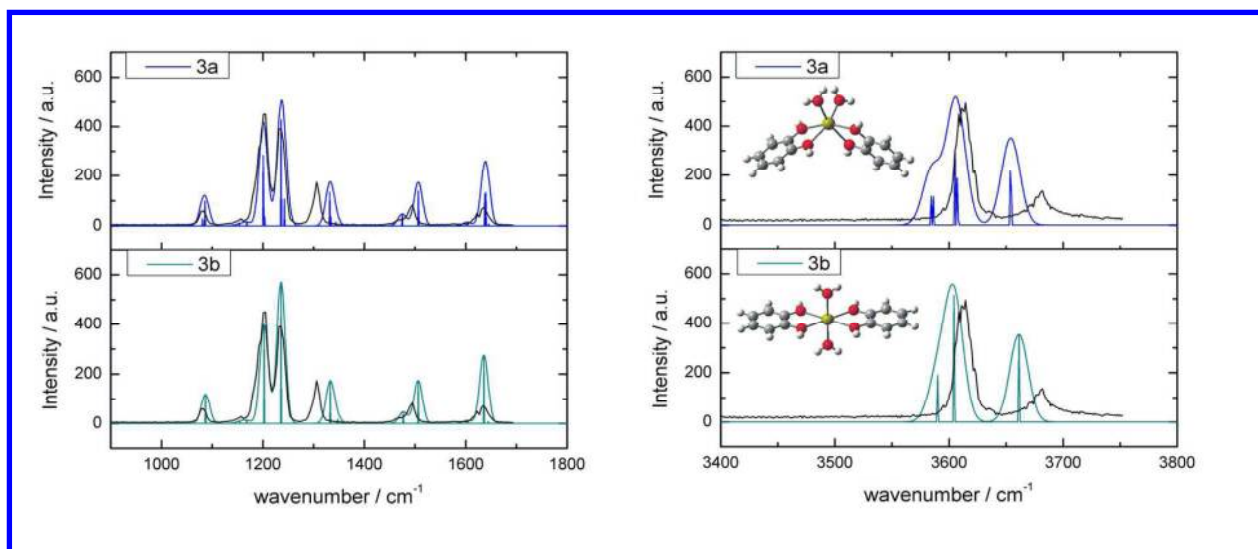
The vibrational assignments of the most stable calculated structures (**2b**, **3a** and **3b**) are listed in Table S3 (see Supporting Information). In general, the deviations of the positions of the experimental band maxima from the frequencies of the most intense mode contributing to the band were less than 20 cm^{-1} in the fingerprint and hydroxyl stretching regions, confirming the vibrational assignments.

The band of the IRMPD spectra near 1300 cm^{-1} exhibited the highest deviations between the experimental and calculated absorption frequencies. The mode (**v_{15}**) appearing in this region has been previously termed as "troublesome" in connection with studies performed with phenol[63]. In this mode, which has predominant contributions from C-C stretching vibrations, the molecule is distorted in the plane, leading to one of the Kekule structures of the benzene ring, thus markedly altering the electron density between carbon atoms. Curiously, upon comparing the IRMPD spectra of salicylate calcium complexes[16] with IR spectra calculated using several DFT functionals and various basis sets, the major deviations were also observed in the region close to 1300 cm^{-1}. However, the choice of the B3LYP functional and 6-311+G(d,p) showed the best

compromise between accurate prediction and low computational cost, which supports as well our choice for the catechol system.

When comparing the assignments of the vibrational modes previously made considering the bare catechol ligand (Table 2) with those predicted by the most stable structures (Table S3 in Supporting Information) it may be seen that the assignments are consistent except for a minor peak (I) appearing at 1160 cm^{-1} for $[Ca(catechol)_2(H_2O)_2]^{2+}$, where the carbon stretching mode identity is different. This difference is not unexpected as this peak (I) is characteristic of the most stable conformer **1a** (Table 1), which actually does not correspond to the structure adopted by catechol upon calcium complexation. Nevertheless, at a first order, tentative assignments from the direct comparison of the bare ligand infrared spectrum are quite satisfactory as they afford nearly the same conclusions as those arisen from the calculated structures.

Overall, the calculated spectra predict well the main features observed in the IRMPD spectra allowing the structural characterization of the cluster ions. Under our experimental conditions, the experimental IRMPD spectrum nicely matches with the predicted IR absorption spectrum for the lowest energy structure, which was characterized for showing the highest possible coordination number on the metal and the catechol behaving as a bidentate ligand with no evidence for *keto*-enol tautomerization.

3.4 Dissociation pathways of $[Ca(catechol)_2(H_2O)]^{2+}$ cluster ions

Exploratory theoretical calculations were performed in order to bring some insights into the relevant ionic structures involved in the dissociation of the doubly charged cluster ions. Among the ions exhibited in the mass spectrum (Figure 1), the cluster ion $[Ca(catechol)_2(H_2O)]^{2+}$ was chosen as a model for being the simplest representative of the group. As previously indicated, the

IRMPD spectrum of the adduct ion $[Ca(catechol)_2(H_2O)]^{2+}$ is well reproduced by the structure **2a**, which was consequently taken as the starting point of all possible fragmentation mechanisms. A full geometry optimization was performed to characterize the transition states, intermediates and primary product ions of the major dissociation reactions from this adduct ion. Frequency analysis of the stationary structures obtained was performed to complete the characterization.

The mechanisms considered with origin in the structure **2a** were of two types (See Scheme 1), neutral ligand losses like water or a catechol ligand (pathways **A** and **B**, respectively) and charge separations in which the dication splits into two monocations. Among the latter, the mechanism explored is the one leading through proton transfer to form protonated catechol and $[Ca(catechol)(H_2O)-H]^+$, denoted pathway **C**. The energy profiles for the structures corresponding to stationary points along the major dissociation pathways by the studied mechanisms are shown in Figure 7. The most significant geometry parameters of the stationary points of the water loss (**A**), catechol loss (**B**) and charge separation (**C**) pathways from the $[Ca(catechol)_2(H_2O)]^{2+}$ ground state structure calculated at the B3LYP levels with a 6-311+G(d,p) basis set are provided in Figure S2 in Supporting Information.
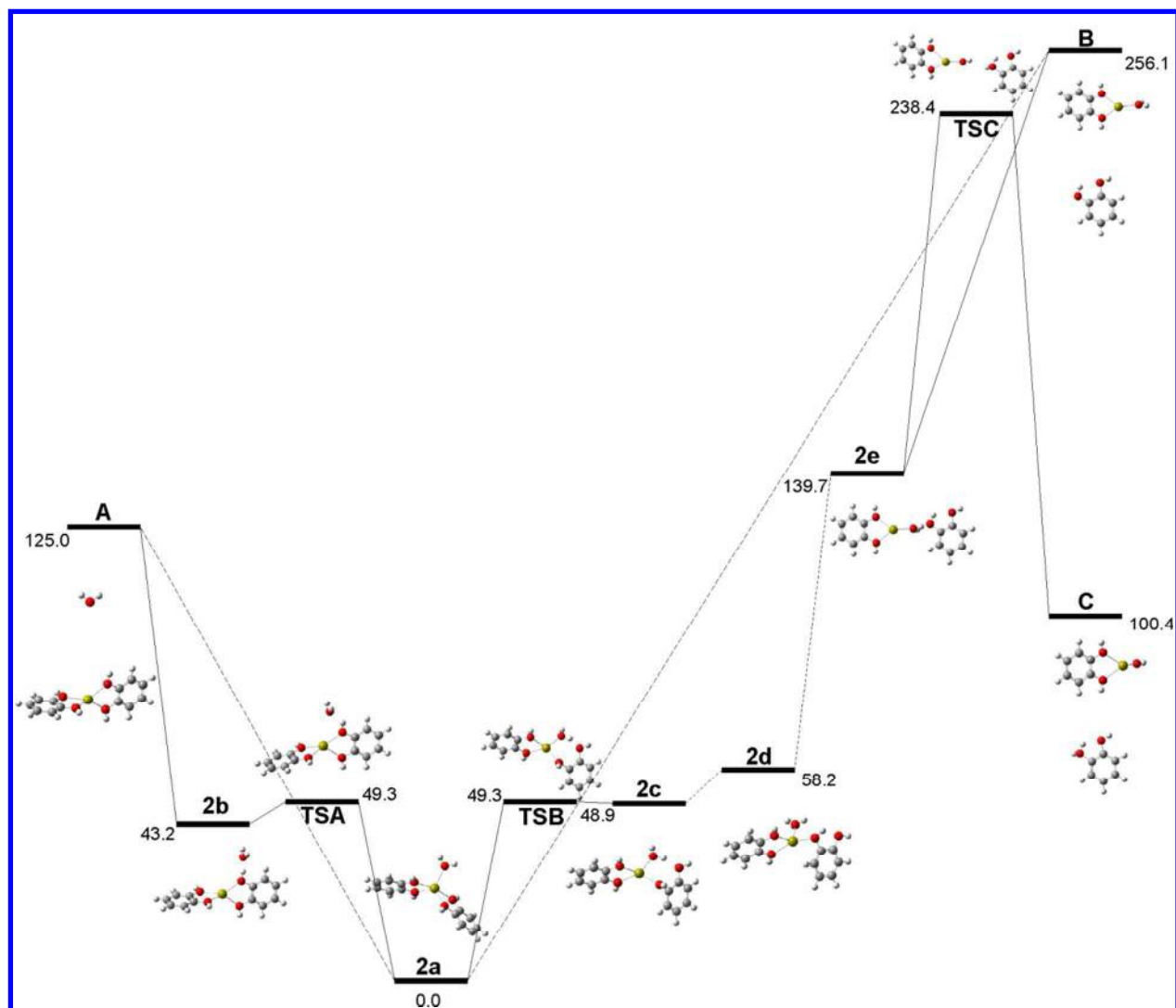
Figure 7. Energy profiles for $[Ca(catechol)_2(H_2O)]^{2+}$ and their interconnecting structures and primary dissociation products for neutral ligand losses and charge separation pathways calculated at the B3LYP/6-311+G(d,p) level of theory. Energies in kJ mol^{-1} including zero-point energy corrections are shown for all structures corresponding to stationary points.

As shown in Figure 7, water loss is the less energetic fragmentation channel as previously observed in the IRMPD experiments. The threshold value calculated is in agreement with that measured for the analogous $Ca(H_2O)_5^{2+}$ complex[64]. The catechol loss and charge separation processes require the transfer of a catechol molecule from the inner solvent shell to the second

solvent shell, where it binds through a single hydrogen bond to the water molecule forming the intermediate **2e**. As separation from calcium occurs, a proton might be transferred from the water molecule to the second solvent shell catechol molecule, thereby allowing formation of two singly charged ions that separate from one another by coulombic repulsion through **TSC**. The geometric parameters of this structure (Figure S2 in Supporting information) resulted similar to those found in the analogous structure calculated[65] from $[Ca(H_2O)_2]^{2+}$, although slightly higher separation distances were found here, probably due to the additional stabilization by the catechol ligand chelating calcium.

The similarity of the energetic barriers for charge separation and neutral loss of catechol from the complex $[Ca(catechol)_2(H_2O)]^{2+}$, are consistent with the generation of the product ions $[Ca(catechol)(OH)]^+$, $[(catechol)H]^+$ (pathway **C**) and $[Ca(catechol)(H_2O)]^{++}$ (pathway **B**) upon CID fragmentation of the former complex (Figure 1b). On the other hand, the calculated value for formation of products of pathway **B** is close to the measured energetic values reported[64] for the loss of two water molecules from the analogous $Ca(H_2O)_5^{2+}$ complex. Thus, the calculated energy threshold values for calcium catechol complexes dissociation pathways were successfully correlated with those available in the literature experimentally measured for doubly charged calcium water complexes.

4. Conclusions

The structures in the gas phase of microhydrated calcium(II) catechol clusters were elucidated using a combination of Collision Induced Dissociation, IRMPD spectroscopy and quantum chemical calculations. Comparison of the IRMPD spectra and calculated IR absorption spectra of various structures yielded good agreement allowing the assignment of spectral features and

hence of the structural motifs. It is shown in particular that the lowest energy structures of mono- and di-hydrated $[Ca(catechol)_2]^{2+}$ were formed under our experimental conditions. The observed IRMPD features clearly show that no *keto*-enol tautomerization is induced upon complexation of catechol to Ca(II). It should be noted, however, that theory suggests that for smaller cluster sizes such as $[Ca(catechol)]^{2+}$, complexes of keto and enol tautomers are quasi-isoenergetic and could thus coexist in the gas phase. Unfortunately, these strongly bound complexes were not amenable for IR spectroscopy under our experimental conditions. The small spectral shifts observed upon addition of a water molecule to $[Ca(catechol)_2(H_2O)]^{2+}$ are consistent with the increase of the coordination number of the metal.

Upon collision induced dissociation of $[Ca(catechol)_2(H_2O)]^{2+}$, mainly doubly charged ions by neutral losses of water and/or a catechol ligand as well as singly charged ions produced by charge separation processes were observed. Quantum chemical calculations at the B3LYP/6-311+G(d,p) level of theory showed that loss of the water molecule was the lowest energy fragmentation channel followed by charge separation products and neutral loss of one catechol molecule, in agreement with the products observed upon CID.

When comparing the assignments of the vibrational modes of microhydrated calcium(II) catechol clusters with those of the bare catechol, an almost perfect match was observed. Thus, the most relevant peaks for structural characterization were those assignable to the stretching and bending modes of the C-O bonds, which appear slightly red-shifted respect to those of the bare catechol. The good agreement between calculated IR spectra highlights the importance of IRMPD spectroscopy as a valuable tool to understand the structure of molecules observed under mass spectrometric conditions.

ACKNOWLEDGMENT

30

SUPPORTING INFORMATION AVAILABLE

Further details on the identity of the species observed in the mass spectra along with their measured *m/z* and error in ppm, the vibrational assignments of the most stable calculated structures, the optimized structures of the calcium complexes containing a single catechol ligand along with their relative energies and calculated IR spectra, and the geometries of the stationary points found in the dissociation pathways may be found in the Supporting Information. This material is available free of charge via the Internet at http://pubs.acs.org.

REFERENCES

(1)　Cheng, H. H.; Haider, K.; Harper, S. S. Catechol and Chlorocatechols in Soil: Degradation and Extractability. *Soil Biol. Biochem.* **1983**, *15*, 311-317.

(2)　Schweigert, N.; Zehnder, A. J. B.; Eggen, R. I. L. Chemical Properties of Catechols and their Molecular Modes of Toxic Action in Cells, from Microorganisms to Mammals. *Environ. Microbiol.* **2001**, *3*, 81-91.

(3)　Pierpont, C. G.; Lange, C. W. The Chemistry of Transition Metal Complexes Containing Catechol and Semiquinone Ligands. *Prog. Inorg. Chem.* **2007**, *41*, 331–442.

(4)　Giroux, S.; Aury, S.; Rubini, P.; Parant, S.; Desmurs, J. -R.; Dury, M. A Spectroscopic Investigation of the Complexing Ability of Catecholate or Salicylate Derivatives Towards Aluminium(III). *Polyhedron* **2004**, *23*, 2393-2404.

(5) Sancho, M. I.; Jubert, A. H.; Blanco, S. E.; Ferretti, F. H.; Castro, E. A. Effects of the Solvent and Temperature on the 2:1 Catechol-Al(III)-Complex. *Spectrochim. Acta, Part A* **2007**, *68*, 387-393.

(6) Whitcomb, D. R.; Rajeswaran, M. The First Silver Catechol Complexes: Crystal Structures of Triphenylphosphine Stabilized Silver Tetra-Bromo and Tetra-Chloro-Catechols. *Polyhedron* **2006**, *25*, 2033-2038.

(7) Brückner, C.; Caulder, D. L.; Raymond, K. N. Preparation and Structural Characterization of Nickel(II) Catecholates. *Inorg. Chem.* **1998**, *37*, 6759-6764.

(8) Lapouge, C.; Cornard, J. -P. Theoretical Study of the Pb(II)-Catechol System in Dilute Aqueous Solution: Complex Structure and Metal Coordination Sphere Determination. *J. Mol. Struct.* **2010**, *969*, 88-96.

(9) Elhabiri, M.; Carrër, C.; Marmolle, F.; Traboulsi, H. Complexation of Iron(III) by Catecholate-Type Polyphenols. *Inorg. Chim. Acta* **2007**, *360*, 353-359.

(10) Lebedev, A. V.; Ivanovo, M. V.; Timoshin, A. A.; Ruuge, E. K. Effect of Calcium Cations on Acid-Base Properties and Free Radical Oxidation of Dopamine and Pyrocatechol. *Biomed. Khim.* **2008**, *54*, 687-695.

(11) Lebedev, A. V.; Ivanova, M. V.; Ruuge, E. K. Calcium-Dioxolene Complexes: Rate Constants of Pyrocatechol Oxidation in the Presence of Ca 2+. *Biophysics* **2011**, *56*, 188-193.

(12) Turecek, F.; Gatlin, C. L. Electrospray Ionization of Inorganic and Organometallic Complexes. In *Electrospray Ionization Mass Spectrometry: Fundamentals, Instrumentation, and Applications,* Cole, R. B., Ed.; Wiley, New York, 1997.

(13) MacAleese, L.; Maître, P. Infrared Spectroscopy of Organometallic Ions in the Gas Phase: From Model to Real World Complexes. *Mass Spectrom. Rev.* **2007**, *26*, 583-605.

(14) Lagutschenkov, A.; Sinha, R. K.; Maître, P.; Dopfer, O. Structure and Infrared Spectrum of the Ag^+-Phenol Ionic Complex. *J. Phys. Chem. A* **2010**, *114*, 11053-11059.

(15) Lagutschenkov, A.; Lorenz, U. J.; Dopfer, O. IR Spectroscopy of Isolated Metal-Organic Complexes of Biocatalytic Interest: Evidence for Coordination Number Four for $Zn^{2+}(imidazole)_4$. *Int. J. Mass Spectrom.* **2011**, *308*, 316-329.

(16) Dain, R. P.; Gresham, G.; Groenewold, G. S.; Steill, J. D.; Oomens, J.; Van Stipdonk, M. J. Infrared Multiple-Photon Dissociation Spectroscopy of Group II Metal Complexes with Salicylate. *Rapid Commun. Mass Spectrom.* **2011**, *25*, 1837-1846.

(17) Sinha, R. K.; Nicol, E.; Steinmetz, V.; Maître, P. Gas Phase Structure of Micro-Hydrated $[Mn(ClO_4)]^+$ and $[Mn_2(ClO_4)_3]^+$ Ions Probed by Infrared Spectroscopy. *J. Am. Soc. Mass Spectrom.* **2010**, *21*, 758-772.

(18) Chiavarino, B.; Crestoni, M. E.; Fornarini, S.; Taioli, S.; Mancini, I.; Tosi, P. Infrared Spectroscopy of Copper-Resveratrol Complexes: A Joint Experimental and Theoretical Study. *J. Chem. Phys.* **2012**, *137*, art. no. 024307.

(19) Dopfer, O.; Lemaire, J.; Maître, P.; Chiavarino, B.; Crestoni, M. E.; Fornarini, S. IR Spectroscopy of Protonated Toluene: Probing Ring Hydrogen Shifts in Gaseous Arenium Ions *Int. J. Mass Spectrom.* **2006**, *249-250*, 149-154.

(20) Dunbar, R. C.; Steill, J. D.; Oomens, J. Encapsulation of Metal Cations by the PhePhe Ligand: A Cation-π Ion Cage. *J. Am. Chem. Soc.* **2011**, *133*, 9376-9386.

(21) Butler, M.; Arroyo Mañez, P.; Cabrera, G. M. Differentiation of Isomeric Hydroxypyridine *N*-Oxides Using Metal Complexation and Electrospray Ionization Mass Spectrometry. *J. Am. Soc. Mass Spectrom.* **2011**, *22*, 545-556.

(22) Butler, M.; Arroyo Mañez, P.; Cabrera, G. M. Proceedings of the 59th ASMS Conference on Mass Spectrometry and Allied Topics, Denver, Colorado, June, 2011.

(23) Bakker, J. M.; Besson, T.; Lemaire, J.; Scuderi, D.; Maître, P. Gas-Phase Structure of a π-Allyl-Palladium Complex: Efficient Infrared Spectroscopy in a 7 T Fourier Transform Mass Spectrometer. *J. Phys. Chem. A* **2007**, *111*, 13415-13424.

(24) Bakker, J. M.; Sinha, R. K.; Besson, T.; Brugnara, M.; Tosi, P.; Salpin, J. -Y.; Maître, P. Tautomerism of Uracil Probed Via Infrared Spectroscopy of Singly Hydrated Protonated Uracil. *J. Phys. Chem. A* **2008**, *112*, 12393-12400.

(25) Bakker, J. M.; Salpin, J. -Y.; Maître, P. Tautomerism of Cytosine Probed by Gas Phase IR Spectroscopy. *Int. J. Mass Spectrom.* **2009**, *283*, 214-221.

(26) Oomens, J.; Sartakov, B. G.; Meijer, G.; von Helden, G. Gas-Phase Infrared Multiple Photon Dissociation Spectroscopy of Mass-Selected Molecular Ions. *Int. J. Mass Spectrom.* **2006**, *254*, 1-19.

(27) Frisch, M. J.; et al. *Gaussian 03*, Revision C. 02. Gaussian, Inc, Wallingford, 2004.

(28) Becke, A. D. Density-Functional Thermochemistry. III. The Role of Exact Exchange. *J. Chem. Phys.* **1993**, *98*, 5648-5652.

(29) Lee, C.; Yang, W.; Parr, R. G. Development of the Colle-Salvetti Correlation-Energy Formula into a Functional of the Electron Density. *Phys. Rev. B: Condens. Matter* **1988**, *37*, 785-789.

(30) Corral, I.; Mó, O.; Yáñez, M.; Scott, A. P.; Radom, L. Interactions between Neutral Molecules and Ca2+: An Assessment of Theoretical Procedures. *J. Phys. Chem. A* **2003**, *107*, 10456-10461.

(31) Alcami, M.; Gonzalez, A. I.; Mó, O.; Yáñez, M. Performance of Density Functional Theory Methods for the Treatment of Metal-Ligand Dications. *Chem. Phys. Lett.* **1999**, *307*, 244-252.

(32) Suárez, D.; Rayón, V. M.; Díaz, N.; Valdés, H. Ab Initio Benchmark Calculations on Ca(II) Complexes and Assessment of Density Functional Theory Methodologies. *J. Phys. Chem. A* **2011**, *115*, 11331-11343.

(33) Halls, M. D.; Velkovski, J.; Schlegel, H. B. Harmonic Frequency Scaling Factors for Hartree-Fock, S-VWN, B-LYP, B3-LYP, B3-PW91 and MP2 with the Sadlej pVTZ Electric Property Basis Set. *Theor. Chem. Acc.* **2001**, *105*, 413-421.

(34) Bythell, B. J.; Hernandez, O.; Steinmetz, V.; Paizs, B.; Maître, P. Tyrosine Side-Chain Catalyzed Proton Transfer in the YG a_2 Ion Revealed by Theory and IR Spectroscopy in

the 'Fingerprint' and XH (X = C, N, O) Stretching Regions. *Int. J. Mass Spectrom.* **2012**, *316-318*, 227-234.

(35) Kohler, M.; Leary, J. A. Gas-Phase Reactions of Doubly Charged Alkaline Earth and Transition Metal Complexes of Acetonitrile, Pyridine, and Methanol Generated by Electrospray Ionization. *J. Am. Soc. Mass Spectrom.* **1997**, *8*, 1124-1133.

(36) Corral, I.; Mó, O.; Yáñez, M.; Salpin, J.-Y.; Tortajada, J.; Radom, L. Gas-Phase Reactions between Urea and Ca^{2-}: The Importance of Coulomb Explosions. *J. Phys. Chem. A* **2004** *108*, 10080-10088.

(37) Trujillo, C.; Mó, O.; Yáñez, M.; Salpin, J. -Y.; Tortajada. J. Gas-Phase Reactions between Thiourea and Ca^{2+}: New Evidence for the Formation of $[Ca(NH_3)]^{2+}$ and other Doubly Charged Species. *ChemPhysChem* **2007**, *8*, 1330-1337.

(38) Trujillo, C.; Mó, O.; Yáñez, M.; Tortajada, J.; Salpin, J. -Y. Selenourea-Ca^{2+} Reactions in Gas Phase. Similarities and Dissimilarities with Urea and Thiourea. *J. Phys. Chem. B* **2008**, *112*, 5479-5486.

(39) Eizaguirre, A.; Mó, O.; Yáñez, M.; Salpin, J. -Y.; Tortajada, J. Modelling Peptide-Metal Dication Interactions: Formamide-Ca^{2+} Reactions in the Gas Phase. *Org. Biomol. Chem.* **2012**, *10*, 7552-7561.

(40) Corral, I.; Mó, O.; Yáñez, M.; Salpin, J. -Y.; Tortajada, J.; Moran, D.; Radom, L. An Experimental and Theoretical Investigation of Gas-Phase Reactions of Ca^{2+} with Glycine. *Chem. Eur. J.* **2006**, *12*, 6787-6796.

(41) Trujillo, C.; Lamsabhi, A.M.; Mó, O.; Yáñez, M.; Salpin, J. -Y. Unimolecular Reactivity upon Collision of Uracil-Ca^{2+} Complexes in the Gas Phase: Comparison with Uracil-M^+ (M = H, alkali metals) and Uracil-M^{2+} (M = Cu, Pb) Systems. *Int. J. Mass Spectrom.* **2011**, *306* ,27-36.

(42) Tuytten, R.; Lemiere, F.; Van Dongen, W.; Esmans, E. L.; Witters, E.; Herrebout, W.; Van Der Veken, B.; Dudley, E.; Newton, R. P. Intriguing Mass Spectrometric Behavior of Guanosine under Low Energy Collision-Induced Dissociation: H_2O Adduct Formation and Gas-Phase Reactions in the Collision Cell. *J. Am. Soc. Mass Spectrom.* **2005**, *16*, 1291-1304.

(43) Stein, S. E. Infrared Spectra by NIST Mass Spec Data Center. In *NIST Chemistry WebBook*, NIST Standard Reference Database Number 69, Linstrom, P. J.; Mallard, W. G., (Eds). National Institute of Standards, Technology: Gaithersburg, MD (http://webbook.nist.gov).

(44) Gerhards, M.; Perl, W.; Schumm, S.; Henrichs, U.; Jacoby, C.; Kleinermanns, K. Structure and Vibrations of Catechol and Catechol·$H_2O(D_2O)$ in the S0 and S1 State. *J. Chem. Phys.* **1996**, *104*, 9362-9375.

(45) Gardner, A. M.; Wright, T. G. Consistent Assignment of the Vibrations of Monosubstituted Benzenes. *J. Chem. Phys.* **2011**, 135, art. no. 114305.

(46) Mandado, M.; Grana, A. M.; Mosquera, R. A. Do 1,2-Ethanediol and 1,2-Dihydroxybenzene Present Intramolecular Hydrogen Bond? *Phys. Chem. Chem. Phys.* **2004**, *6*, 4391-4396.

(47) Gomez-Zaleta, B.; Gomez-Balderas, R.; Hernandez-Trujillo, J. Theoretical Analysis of Hydrogen Bonding in Catechol-n(H_2O) Clusters (n = 0...3). *Phys. Chem. Chem. Phys.* **2010**, *12*, 4783-4790.

(48) Shimanouchi, T. Molecular Vibration Frequencies. In *NIST Chemistry WebBook*, NIST Standard Reference Database Number 69, Linstrom, P. J.; Mallard, W. G., (Eds). National Institute of Standards, Technology: Gaithersburg, MD (http://webbook.nist.gov).

(49) O'Brien, J. T.; Williams, E. R. Coordination Numbers of Hydrated Divalent Transition Metal Ions Investigated with IRPD Spectroscopy. *J. Phys. Chem. A* **2011**, *115*, 14612-14619.

(50) Bandyopadhyay, B.; Duncan, M. A. Infrared Spectroscopy of $V^{2+}(H_2O)$ Complexes. *Chem. Phys. Lett.* **2012**, *530*, 10-15.

(51) Walters, R. S.; Pillai, E. D.; Duncan, M. A. Solvation Dynamics in $Ni^+(H_2O)_n$ Clusters Probed with Infrared Spectroscopy. *J. Am. Chem. Soc.* **2005**, *127*, 16599-16610.

(52) Bush, M. F.; Saykally, R. J.; Williams, E. R. Hydration of the Calcium Dication: Direct Evidence for Second Shell Formation from Infrared Spectroscopy. *ChemPhysChem* **2007**, *8*, 2245-2253.

(53) Headrick, J. M.; Diken, E. G.; Walters, R. S.; Hammer, N. I.; Christie, R. A.; Cui, J.; Myshakin, E. M.; Duncan, M. A.; Johnson, M. A.; Jordan, K. D. Chemistry: Spectral Signatures of Hydrated Proton Vibrations in Water Clusters. *Science* **2005**, *308*, 1765-1769.

(54) Pankewitz, T.; Lagutschenkov, A.; Niedner-Schatteburg, G.; Xantheas, S. S.; Lee, Y. -T. Infrared Spectrum of NH_4^+ (H_2O): Evidence for Mode Specific Fragmentation. *J. Chem. Phys.* **2007**, *126*, art. no. 074307.

(55) Lagutschenkov, A.; Langer, J.; Berden, G.; Oomens, J.; Dopfer, O. Infrared Spectra of Protonated Neurotransmitters: Dopamine. *Phys. Chem. Chem. Phys.* **2011**, *13*, 2815-2823.

(56) Salpin, J. -Y.; Guillaumont, S.; Ortiz, D.; Tortajada, J.; Maître, P. Direct Evidence for Tautomerization of the Uracil Moiety within the Pb^{2+}/Uridine-5′Monophosphate Complex: A Combined Tandem Mass Spectrometry and IRMPD Study. *Inorg. Chem.* **2011**, *50*, 7769-7778.

(57) Wang, Y. A Computational Study of Keto-Enol Equilibria of Catechol in Gas and Aqueous Solution Phase. Thesis Submitted to the Graduate Faculty of Wake Forest University for the Degree of M.Sc. in the Department of Chemistry **2009** Winston-Salem, North Carolina.

(58) Lei, X. L.; Pan, B. C. Structures, Stability, Vibration Entropy and IR Spectra of Hydrated Calcium Ion Clusters $[Ca(H_2O)_n]^{2+}$ (n = 1-20, 27): A Systematic Investigation by Density Functional Theory. *J. Phys. Chem. A* **2010**, *114*, 7595-7603.

(59) Jiang, L.; Wende, T.; Bergmann, R.; Meijer, G.; Asmis, K. R. Gas-Phase Vibrational Spectroscopy of Microhydrated Magnesium Nitrate Ions $[MgNO_3(H_2O)_{1-4}]^+$. *J. Am. Chem. Soc.* **2010**, *132*, 7398-7404.

(60) Paterova, J.; Heyda, J.; Jungwirth, P.; Shaffer, C. J.; Revesz, A.; Zins, E. L.; Schroder, D. Microhydration of the Magnesium(II) Acetate Cation in the Gas Phase. *J. Phys. Chem. A* **2011**, *115*, 6813-6819.

(61) Trujillo, C.; Lamsabhi, A. M.; Mó, O.; Yáñez, M.; Salpin, J. -Y. Interaction of Ca^{2+} with Uracil and Its Thio Derivatives in the Gas Phase. *Org. Biomol. Chem.* **2008**, *6*, 3695-3702.

(62) Salpin, J.Y.; Guillaumont, S.; Tortajada, J.; MacAleese, L.; Lemaire, J.; and Maitre, P. Infrared Spectra of Protonated Uracil, Thymine and Cytosine. *ChemPhysChem* **2007**, *8*, 2235-2244.

(63) Michalska, R. D.; Zierkiewicz, W.; Bieńko, D. C.; Wojciechowski, W.; Zeegers-Huyskens, T. "Troublesome" Vibrations of Aromatic Molecules in Second-Order Möller-Plesset and Density Functional Theory Calculations: Infrared Spectra of Phenol and Phenol-OD. *J. Phys. Chem. A* **2001**, *105*, 8734-8739.

(64) Carl, D. R.; Armentrout, P. B. Experimental Investigation of the Complete Inner Shell Hydration Energies of Ca^{2+}: Threshold Collision-Induced Dissociation of $Ca^{2+}(H_2O)_x$ Complexes (x = 2-8). *J. Phys. Chem. A* **2012**, *116*, 3802-3815.

(65) Beyer, M.; Williams, E. R.; Bondybey, V. E. Unimolecular Reactions of Dihydrated Alkaline Earth Metal Dications $M^{2+}(H_2O)_2$, M = Be, Mg, Ca, Sr, and Ba: Salt-Bridge Mechanism in the Proton-Transfer Reaction $M^{2+}(H_2O)_2 \rightarrow MOH^+ + H_3O^+$. *J. Am. Chem. Soc.* **1999**, *121*, 1565-1573.

1
2
3
4
5
6
7
8
9
10
11
12
13
14
15
16
17
18
19
20
21
22
23
24
25
26
27
28
29
30
31
32
33
34
35
36
37
38
39
40
41
42
43
44
45
46
47
48
49
50
51
52
53
54
55
56
57
58
59
60

TABLE OF CONTENTS